chemistry

MDPI

Article

Blue-Emitting 2D- and 3D-Zinc Coordination Polymers Based on Schiff-Base Amino Acid Ligands

Rodavgi Karakousi [1], Pinelopi A. Tsami [1], Maria-Areti I. Spanoudaki [1], Scott J. Dalgarno [2], Vassileios C. Papadimitriou [1,3,4,*] and Constantinos J. Milios [1,*]

[1] Department of Chemistry, The University of Crete, 71003 Herakleion, Greece; chem2077@edu.chemistry.uoc.gr (R.K.); chemp1156@edu.chemistry.uoc.gr (P.A.T.); chemp1166@edu.chemistry.uoc.gr (M.-A.I.S.)
[2] Institute of Chemical Sciences, Heriot-Watt University, Riccarton, Edinburgh EH14 4AS, UK; s.j.dalgarno@hw.ac.uk
[3] Chemical Sciences Laboratory, National Oceanic and Atmospheric Administration, Boulder, CO 80305, USA
[4] Cooperative Institute for Research in Environmental Sciences, University of Colorado, Boulder, CO 80309, USA
* Correspondence: bpapadim@uoc.gr (V.C.P.); komil@uoc.gr (C.J.M.)

Abstract: The solvothermal reaction of $Zn(NO_3)_2 \cdot 4H_2O$, 1-OH-2-naphthaldehyde, and 2-methylalanine (*mAla*) in MeOH leads to the formation of complex $\{[ZnL_1]\}_{2n}$ (**1**) (H_2L_1 = the Schiff-base resulting from the reaction of 1-OH-2-naphthaldehyde and *mAla*) in good yields. The structure of the neutral species, as determined by single-crystal crystallography, describes a two-dimensional coordination polymer, with repeating $\{Zn_2\}$ units bridged by *syn*, *anti*-carboxylate groups of the Schiff-base ligands. Repeating the same reaction using glycine (*gly*) instead of *mAla* leads to the formation of complex $\{[ZnL_2] \cdot 0.33MeOH\}_{3n}$ (**2**.0.33MeOH) (H_2L_2 = the Schiff-base resulting from the reaction of 1-OH-2-naphthaldehyde and *gly*), again in good yields. Complex **2** describes a three-dimensional coordination polymer based on $\{Zn_2\}$ building blocks, arranged by *anti*, *anti*-carboxylate groups in a 3D motif. Complexes **1** and **2** were found to strongly emit at ~435 nm (λ_{exc} = 317 nm) both in solution and solid state, with complex **2** displaying a slightly longer lifetime of τ_{av} = 2.45 ns vs. τ_{av} = 2.02 ns for **1**.

Keywords: Zn coordination polymers; 2D; 3D; amino acid ligands; Schiff-base ligands; crystal structure; fluorescence; fluorescence lifetimes

Citation: Karakousi, R.; Tsami, P.A.; Spanoudaki, M.-A.I.; Dalgarno, S.J.; Papadimitriou, V.C.; Milios, C.J. Blue-Emitting 2D- and 3D-Zinc Coordination Polymers Based on Schiff-Base Amino Acid Ligands. *Chemistry* **2023**, *5*, 1770–1780. https://doi.org/10.3390/chemistry5030121

Academic Editors: Zoi Lada and Konstantis Konidaris

Received: 5 July 2023
Revised: 6 August 2023
Accepted: 7 August 2023
Published: 9 August 2023

1. Introduction

Over the past three decades, since their deliberately targeted synthesis by Professor R. Robson in 1989 [1], metal–organic frameworks (MOFs) have dominated the scientific field of coordination polymers as a captivating emerging class of materials, combining the fields of inorganic and organic chemistry [2,3]. These three-dimensional crystalline coordination polymers have attracted attention due to their exceptional chemical properties, arising from the elegant way of assembling the metal ions or cluster-based building units with suitable organic ligands that act as linkers/bridges. Such species allow for fine-tuning the surface chemistry and customizing the pore size, maximizing the selectivity in adsorption processes. MOFs, due to their unique structure, present outstanding chemical, thermal, and mechanical stability [4], making them highly desirable for a diverse range of applications such as drug delivery [5], biomolecule encapsulation [6], gas storage and separation [7], catalysis and photocatalysis [8], sensing [9], and magnetic properties [10], paving new pathways for advancements in medical and technological applications [11].

The formation, as well as the identity of such polymeric materials, is based on many synthetic parameters affecting the reaction conditions, e.g., reaction time, presence of base and/or auxiliary ligands, and pressure/temperature. However, selecting the crystallization conditions is of great importance since, in many cases, it enables controlling the identity of the isolated products (i.e., kinetic vs. thermodynamic products) [12,13].

Up until now, a wide range of metal ions have been employed for the synthesis of such unique coordination polymers [14], with the most commonly employed being zinc, a $3d^{10}$ transition metal ion. The main reasons for that are: (1) zinc is a highly abundant element in the earth's crust [15], and, as such, it is readily available, ensuring a sustainable supply; and (2) zinc-based starting materials/salts are relatively low-cost [16], thus enhancing the economic feasibility of manufacturing zinc-based MOFs. Furthermore, the low-toxicity of zinc compounds [17–19] is of paramount importance in the context of MOFs' potential biomedical and environmental applications.

Luminescent MOFs are a highly significant sub-class of 3D coordination polymers, since they hold great value as chemical sensors upon combining the porosity of a specific MOF and/or its selectivity towards a guest molecule, along with their inherent luminescent properties [20]. This is particularly crucial since the luminescence characteristics of such MOFs may be potentially modified when exposed to the guest molecule, even in small traces, triggering the sensing sequence. Furthermore, in most cases the emission of the MOFs stems from the organic linker/bridge chromophore; as such, the search for suitable organic chromophore ligands that may promote the formation of 3D coordination polymers is of great importance. With this in mind, we herein report the synthesis and full characterization of two new Zn coordination polymers based upon the Schiff-base ligands H_2L_1 and H_2L_2 (Figure 1).

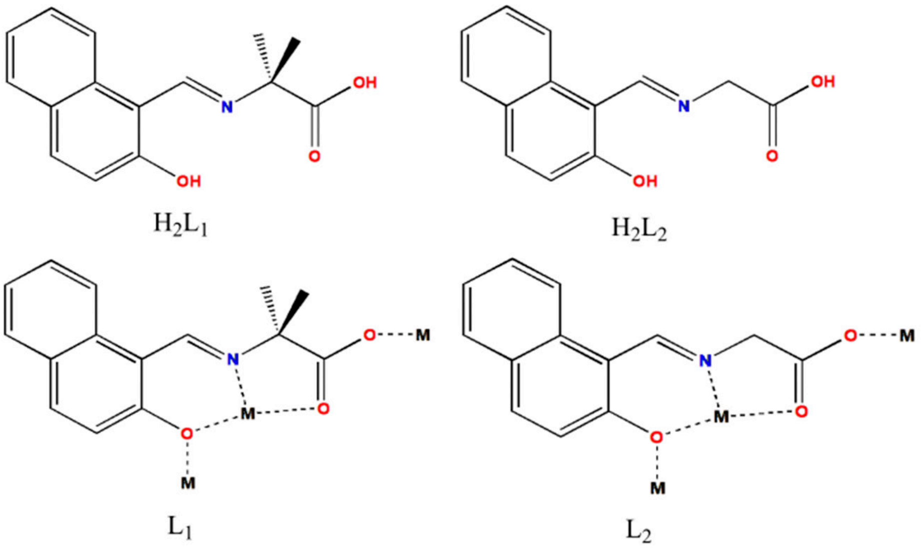

Figure 1. The H_2L_1 and H_2L_2 ligands reported in this work and their coordination modes in **1** and **2**, respectively.

2. Materials and Methods

All chemicals were obtained from commercial suppliers (Sigma-Aldrich, Athens, Greece) and were used without further purification/treatment.

$\{[ZnL_1]\}_{2n}$ (complex **1**):

$Zn(NO_3)_2 \cdot 4H_2O$ (0.130 g, 0.5 mmol), 2-OH-1-napthaldehyde (0.172 g, 1 mmol), and 2-aminoisobutyric acid (0.103 g.; 1 mmol) were heated in Teflon-lined autoclaves with 15 mL MeOH at 120 °C for 12 h. Upon slowly cooling to room temperature, yellow-gold crystals were formed and collected by filtration. Elemental analysis (%) calculated for $C_{15}H_{13}NO_3Zn$ (**1**): C, 56.18; H, 4.09; N, 4.37. Found: C, 56.09; H, 3.97; and N, 4.41. Yield ~40%. FT-ATIR (cm^{-1}): 1625s, 1574vs, 1544s, 1500m, 1462vs, 1404vs, 1331s, 1296s, 1174vs, 1149s, 833vs, 737vs, and 514vs.

$\{[ZnL_2]\cdot 0.33MeOH\}_{3n}$ (complex **2**.0.33MeOH):

Complex **2** was synthesized in an analogous manner to **1**, upon using glycine instead of 2-aminoisobutyric acid. Elemental analysis (%) calculated for $C_{13}H_9NO_3Zn$ (**2**): C, 53.36; H, 3.10; and N, 4.79. Found: C, 53.42; H, 2.98; and N, 4.71. Yield ~40%. FT-ATIR (cm^{-1}): 1622vs, 1602vs, 1573vs, 1542vs, 1510m, 1457s, 1421vs, 1389s, 1327s, 1291vs, 1234s, 1188m, 1166s, 1149w, 1087m, 955s, 841vs, 759s, 746vs, 562s, and 460vs.

2.1. Characterization

Elemental analyses (C, H, and N) were performed by the University of Ioannina microanalysis service. Powder XRD data were collected on freshly prepared samples of **1** and **2** on a PANanalytical X'Pert Pro MPD diffractometer (UoC). FTIR−ATR spectra were recorded on a PerkinElmer FTIR Spectrum BX spectrometer (UoC). Solution UV-Vis spectra were recorded on a double beam Hitachi U-2100 UV-Vis spectrophotometer (UoC). Solid-state and solution fluorescence spectra and lifetimes were determined on a photoluminescence (PL) Edinburgh Instrument FS5 Steady State Spectrometer (UoC). For solution fluorescence spectra, a JASCO FP-8300 spectrofluorometer was also utilized (UoC).

2.2. X-ray Diffraction

Single-crystal X-ray diffraction data were collected on a Bruker D8 VENTURE diffractometer (University of Crete) equipped with a PHOTION II CPAD detector. Data collection parameters and structure solution and refinement details are listed in Table 1. Full details can be found in the CIF files with CCDC reference numbers 2270710 and 2270711, for **1** and **2**, respectively.

Table 1. Crystal data and structure refinement for complexes **1** and **2**.

	1	**2**
Empirical formula	$C_{15}H_{13}NO_3Zn$	$C_{13\cdot 33}H_{10\cdot 33}NO_{3\cdot 33}Zn$
Formula weight	320.63	303.17
Temperature/K	210	210
Crystal system	Moniclinic	Trigonal
Space group	$P2_1/c$	R-3
a/Å	14.5062 (3)	26.7293 (3)
b/Å	9.6958 (2)	26.7293 (3)
c/Å	9.7987 (2)	8.5248 (2)
α/°		
β/°	107.697 (1)	
γ/°		120
Volume/Å^3	1312.96 (5)	5274.61 (17)
Z	4	18
ρ_{calc} g/cm^3	1.622	1.718
μ/mm^{-1}	2.660	2.962
F(000)	656.0	2771.0
Crystal size/mm^3	0.32 × 0.30 × 0.24	0.28 × 0.22 × 0.20
Radiation	CuKα (λ = 1.54178)	CuKα (λ = 1.54178)
2Θ range for data collection/°	11.148 to 139.594	6.614 to 139.834
Index ranges	$-17 \leq h \leq 17, -11 \leq k \leq 11,$ $-11 \leq l \leq 11$	$-31 \leq h \leq 32, -31 \leq k \leq 20,$ $-10 \leq l \leq 10$
Reflections collected	14,311	7111
Independent reflections	2464	2214

Table 1. *Cont.*

	1	**2**
Data/restraints/parameters	2464/0/183	2214/0/163
Goodness-of-fit on F^2	1.062	1.051
Final *R* indexes ($I \geq 2\sigma$ (I))	$R_1 = 0.0219$, $wR_2 = 0.0580$	$R_1 = 0.0243$, $wR_2 = 0.0603$
Final *R* indexes (all data)	$R_1 = 0.0233$, $wR_2 = 0.0592$	$R_1 = 0.0278$, $wR_2 = 0.0626$
Largest diff. peak/hole/e $Å^{-3}$	0.31/−0.26	0.27/−0.30

3. Results and Discussion

3.1. Synthesis and Crystal Structures

The 1:2:2 solvothermal reaction of $Zn(NO_3)_2O_3)_2 \cdot 4H_4H_2O$, 1-OH-2-naphthaldehyde, and *mAla* in MeOH forms complex $\{[ZnL_1]\}_{2n}$ (**1**) in good yields. With the structure of complex **1** established via single-crystal X-ray crystallography (vide infra) we investigated various synthetic parameters as a means of modifying the identity of the complex. However, upon changing the metal to ligand ratio, in the presence/absence of various bases (i.e., NEt_3, CH_3ONa), and using various zinc salts (i.e., $ZnSO_4$ and $Zn(OAc)_2.2H_2O$) we were not able to isolate any crystalline material different to **1**, as evidenced by pXRD comparison. Furthermore, all attempts to isolate any crystalline material upon normal laboratory conditions (i.e., aerobic conditions at room temperature) proved fruitless, since, in all cases, a sticky yellowish slurry was formed upon slow evaporation of the solvent [21].

Our next goal was to investigate whether the nature of the Schiff-base formed in situ could affect the identity and/or the dimensionality of the product; therefore, we employed the amino acid *gly* instead of *mAla*, and from the analogous solvothermal reaction of $Zn(NO_3)_2O_3)_2 \cdot 4H_4H_2O$, 1-OH-2-naphthaldehyde, and *gly* in MeOH we were able to isolate complex $\{[ZnL_2] \cdot 0.33MeOH\}_{3n}$ (**2**.0.33MeOH) in good yields. To our great surprise, complex **2** describes a 3D-coordination polymer as was established by single-crystal X-ray crystallography (vide infra), thus establishing the leading role of the Schiff-base in dictating the dimensionality of the products. Furthermore, given that the two Schiff-base ligands, H_2L_1 and H_2L_2, differ only in the nature of amino acid employed, *mAla* in **1** vs. *gly* in **2**, it becomes apparent that the change from 2D to 3D (from **1** to **2**) should be attributed in the nature/structure/properties of the amino acid ligand employed. Given that both amino acid ligands display very similar pKa values (2.36 and 2.35, for *mAla* and *gly*, respectively), we may safely assume that the acidity of the amino acid ligand does not hold a pivotal role in dictating the dimensionality of the products, suggesting that other factors, i.e., steric hindrance, may govern the formation of the products.

Single-crystal X-ray diffraction studies of **1** reveal that complex **1** crystallizes in the centrosymmetric monoclinic space group $P2_1/c$ (Figure 2). Its asymmetric unit (ASU) contains one crystallographically independent zinc centre bound to one dianionic $L_1{}^{2-}$ ligand. Each $L_1{}^{2-}$ ligand adopts a η^2: η^1: η^1: η^1: μ_3 coordination mode, forming a six-member chelate ring around each metal centre, while bridging to two neighboring Zn centres via the alkoxide group and one $O_{carboxylate}$ atom. Furthermore, the carboxylate unit of the amino acid part of the $L_1{}^{2-}$ ligands adopts a *syn, anti-* η^1: η^1: μ coordination mode, bridging two Zn metal ions at ~5.59 Å. Each Zn^{II} ion displays a slightly distorted square-pyramidal $\{O_4N\}$ geometry ($\tau = 0.31$) [22]. Alternatively, the structure may be described as consisting of $\{Zn_2(L_1{}^{2-})_2\}$ dimers, in which the metal atoms are connected through the μ-$O_{alkoxide}$ groups of the $L_1{}^{2-}$ ligands. The Zn · · · Zn distance within each dimer is ~3.17 Å, while neighboring $\{Zn_2\}$ are located at ~5.59 Å linked via the *syn, anti-* η^1: η^1: μ carboxylate groups of the $L_1{}^{2-}$ ligands.

The overall packing of the **1** describes a 2D layered-based network (Figure 3), in which neighboring 2D layers are stacked at a distance of ~14.5 Å (closest Zn···Zn distance), stabilized via inter-layer C-H . . . π interactions, at ~3.73 Å.

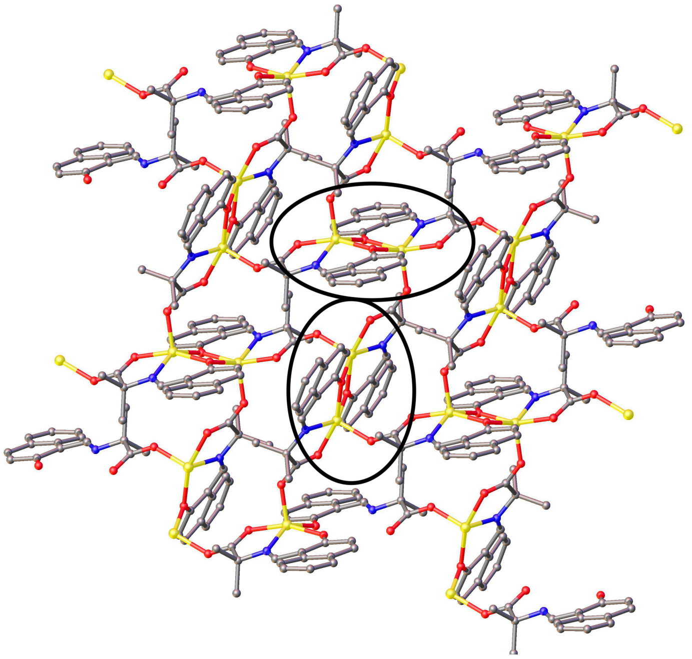

Figure 2. The crystal structure of **1** viewed on the *bc* plane, highlighting the formation of $\{Zn_2\}$ units. Colour code: Zn^{II} = yellow; O = red; N = blue; and C = grey. H-atoms are omitted for clarity.

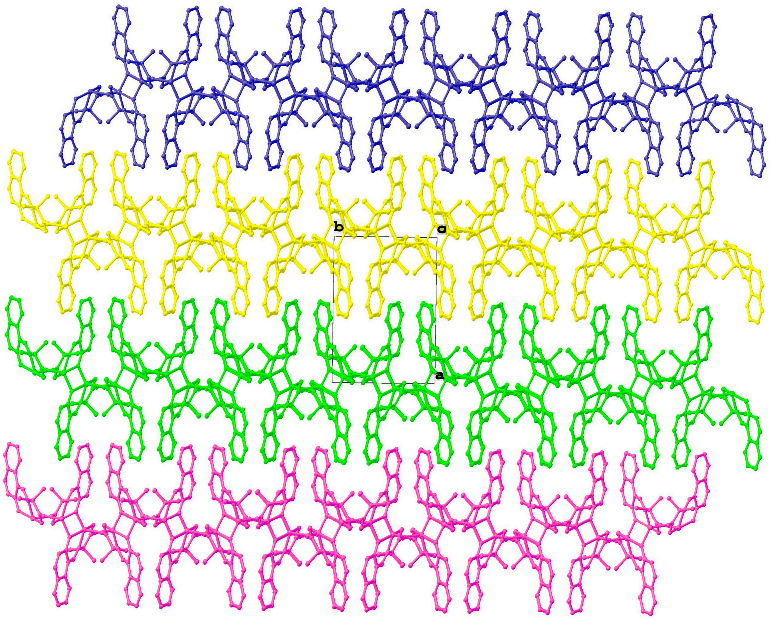

Figure 3. The crystal packing of **1** viewed on the *ab* plane. Different layers are depicted in different colours. H-atoms are omitted for clarity.

Complex **2** crystallizes in the trigonal space group *R*-3, forming a 3D framework (Figure 4). Its ASU contains one crystallographically independent zinc centre bound to one dianionic L_2^{2-} ligand found in a η^2: η^1: η^1: η^1: μ_3 coordination mode, forming a six-member chelate ring around each metal centre, while bridging to two neighboring Zn centres via the alkoxide group and one $O_{carboxylate}$ atom, as observed for L_1^{2-} in **1**. However, the carboxylate unit of the amino acid part of the L_1^{2-} ligands now adopts a *anti, anti-* η^1: η^1: μ coordination mode vs. the *syn, anti-* η^1: η^1: μ mode found in **1**, which we believe is the main reason for the different dimensionality between **1** and **2**. Again, as in **1**, the zinc ions are five-coordinate, but now are found in a severely distorted (τ = 0.46) square-pyramidal $\{O_4N\}$ environment. In the extended structure of **2**, cylindrical channels are running along the *c* axis, formed by the aromatic rings of L_2^{2-}, resulting in a solvent-accessible volume of ~531 $Å^3$ per unit cell (~10.1% of the unit cell volume).

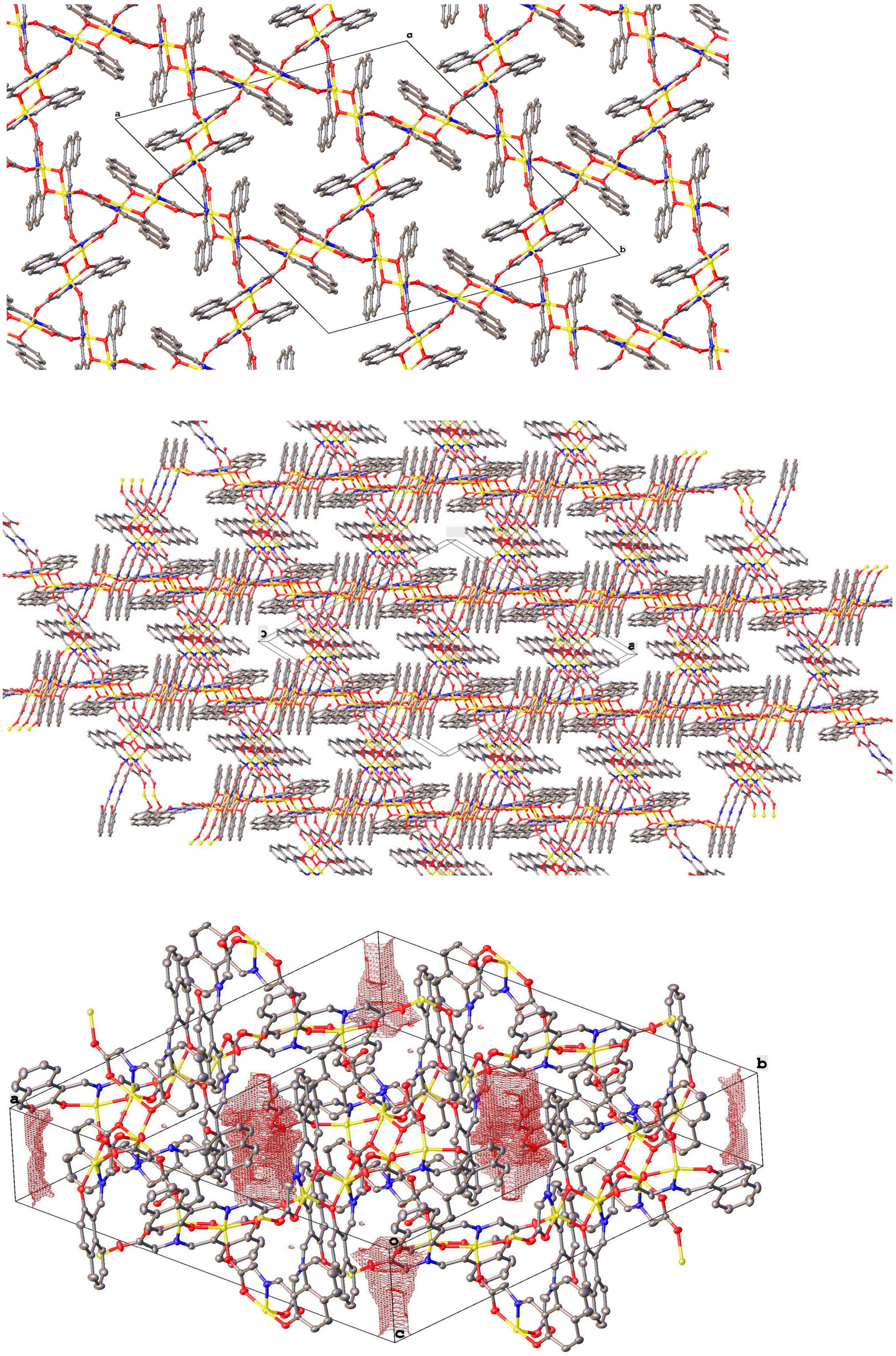

Figure 4. The crystal structure of **2** viewed down the *c* axis (**top**), its extended structure (**middle**) and the channels running down *c* axis (**bottom**). Colour code: the same as in Figure 2. H-atoms are omitted for clarity.

As in **1**, $\{Zn_2(L_2^{2-})_2\}$ dimers are present in the structure serving as building units, in which the metal atoms are linked via the μ-$O_{alkoxide}$ groups of the L_2^{2-} ligands. The Zn $\cdots$ Zn distance within each dimer is ~3.15 Å, while neighboring $\{Zn_2\}$ are located at ~5.64 Å linked via the *anti, anti-* η^1: η^1: μ carboxylate groups of the L_2^{2-} ligands. However, a comparison between the $\{Zn_2\}$ building units in **1** and **2** reveals that, although the $\{Zn_2(O_R)_2\}$ metallic core of each dimer is planar in both cases, the relative orientation of the planar aromatic rings with the respect to the $\{Zn_2(O_R)_2\}$ plane differs; more specifically, in **1** the angle between the naphthalene aromatic ring and the $\{Zn_2(O_R)_2\}$ plane is 21.7°, while in **2** the angle was found ~40.6°.

3.2. Optical Properties

Figure 5 shows the UV-Vis spectra recorded for methanolic solutions of complexes **1** and **2**, between 200 and 425 nm. The purity of the samples was verified by means of pXRD comparison to their theoretical patterns (Figure S2).

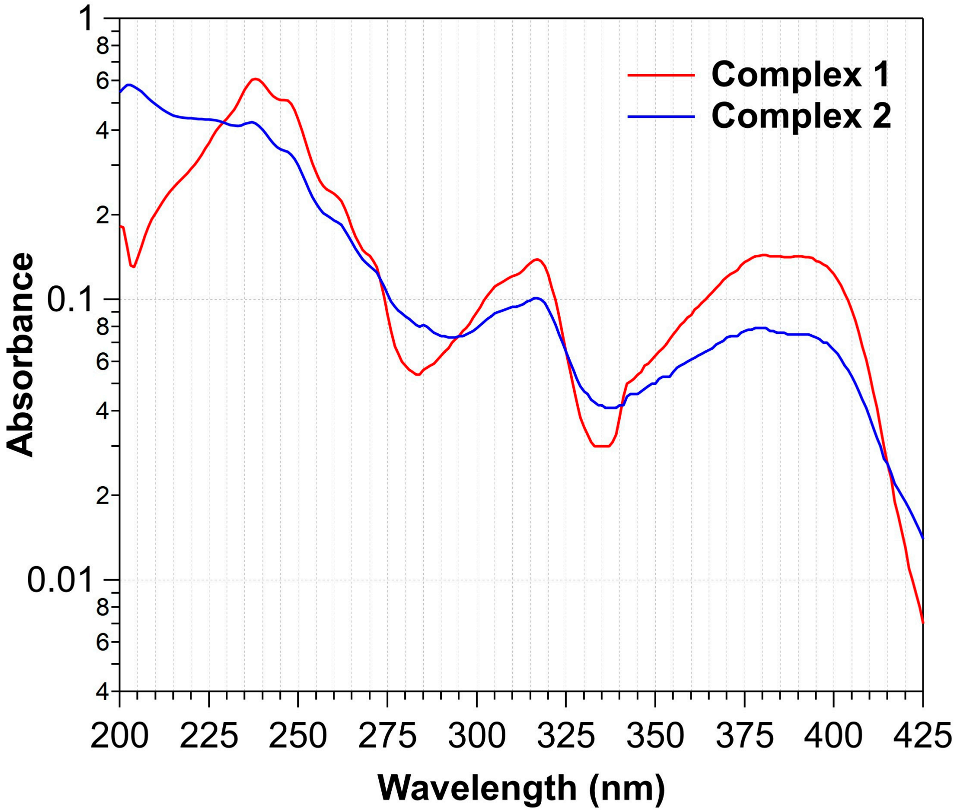

Figure 5. UV-Vis absorption spectra recorded for complexes **1** and **2**.

Three main bands (metal-to-ligand charge transfer, MLCT) are observed for both complexes, with peak maxima at 238 (b_1), 317 (b_2), and 380 (b_3) nm, among which the band at 238 nm was found to be the strongest. In addition, vibrational structure was observed in all the absorption bands, that was identical in shape and wavelength positioning for both complexes. Furthermore, the similar features of the UV-Vis absorption spectra reveal the presence of the same chromophore in the species, as expected from their crystal structures. The only significant difference between the UV-Vis absorption spectra of complexes **1** and **2** lies on the reversed trend in absorbance relative intensity between bands b_2 and b_3, with b_2 being stronger for complex **1** and weaker for complex **2**. The UV-Vis absorption spectra recorded for the two pretreated solutions of the complexes were utilized to measure the fluorescence spectra of the complexes. In particular, the fluorescence spectra of solutions **1** and **2** were measured at excitation wavelengths, for which the absorbance values were equal for the two complexes, i.e., 229, 273, and 325 nm. Note that the solution fluorescence spectra for the two complexes were also recorded at the b_2 maximum absorbance, 317 nm, as well as their excitation spectra using λ_{em} = 441 nm (Figure S3). In Figure 6 the solution steady-state fluorescence spectra of **1** and **2** are displayed, using as excitation energy the three wavelengths at which complexes **1** and **2** absorb equally.

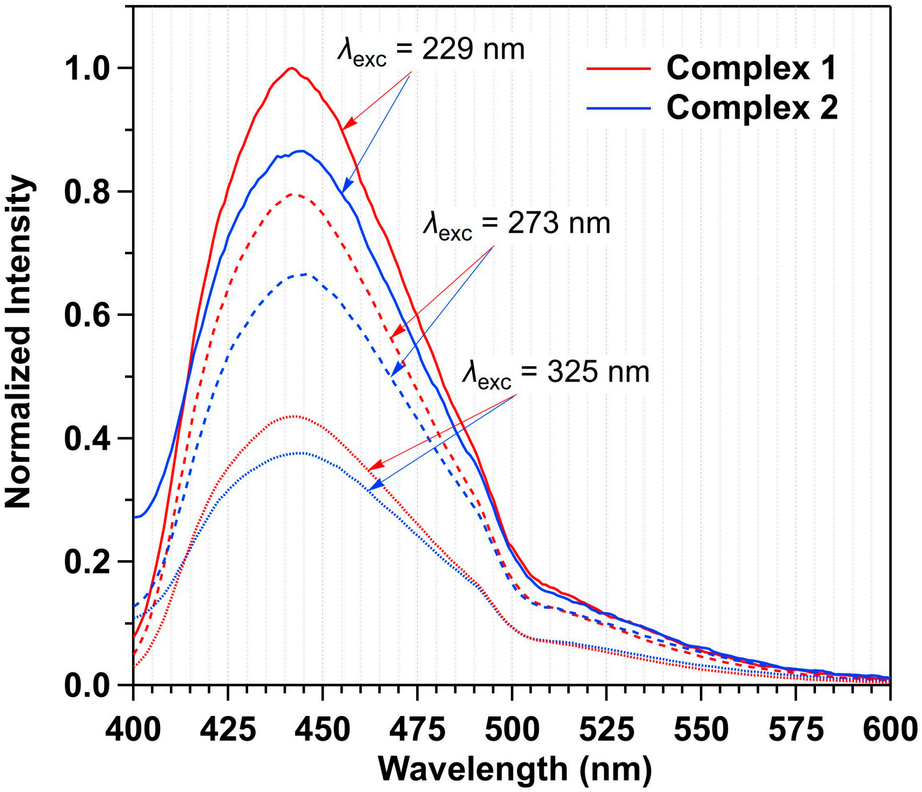

Figure 6. Solution normalized fluorescence spectra of complexes **1** and **2**, recorded with excitation wavelengths 229, 273, and 325 nm, at which UV-Vis absorbance values for the two species were measured to be equal.

Although shape-wise the fluorescence spectra of the two complexes are very similar, a slight, but systematic red-shift of the fluorescence maximum intensity was observed, in the case of complex **2**, with $\lambda_{1,max}$ and $\lambda_{2,max}$ to be at 442 and 445 nm, respectively. Further, the ~15% lower fluorescence intensity observed for complex **2,** at the three different excitation wavelengths where the absorbance was equal, indicates that for complex **1** the fluorescence probability is higher, in excellent agreement with its smaller fluorescence lifetime (*vide infra*). Figure 7 shows the solid-state fluorescence spectra recorded at excitation wavelength λ_{exc} = 317 nm, for **1** and **2**; again, the two fluorescence spectra are very similar, and present great similarity to those in solution. However, in the solid-state the intensity maxima occur at shorter wavelengths, ~435 nm, as anticipated since the effect of solvent relaxation, i.e., solvent molecules reorientation around the excited-state dipole, effectively lowers the energy and shifts the fluorescence to longer wavelengths.

The solid-state fluorescence of 1-OH-2-naphthaldehyde was also recorded for comparison purposes (Figure S4) using 317 nm as excitation wavelength, and it can be observed that its maximum fluorescence signal, λ_{max} = 451 nm, is substantially blue-shifted, ~16 nm, in **1** and **2**. Finally, solid-state fluorescence lifetimes for **1** and **2** were also measured using the output of a pulsed picosecond diode laser (375 ± 10 nm) as excitation wavelength and are presented in Figure 8. The fluorescence decay was fitted to a double-exponential kinetic expression, yielding two decay times for each complex, in consistence with multiple conformational states for each complex [23].

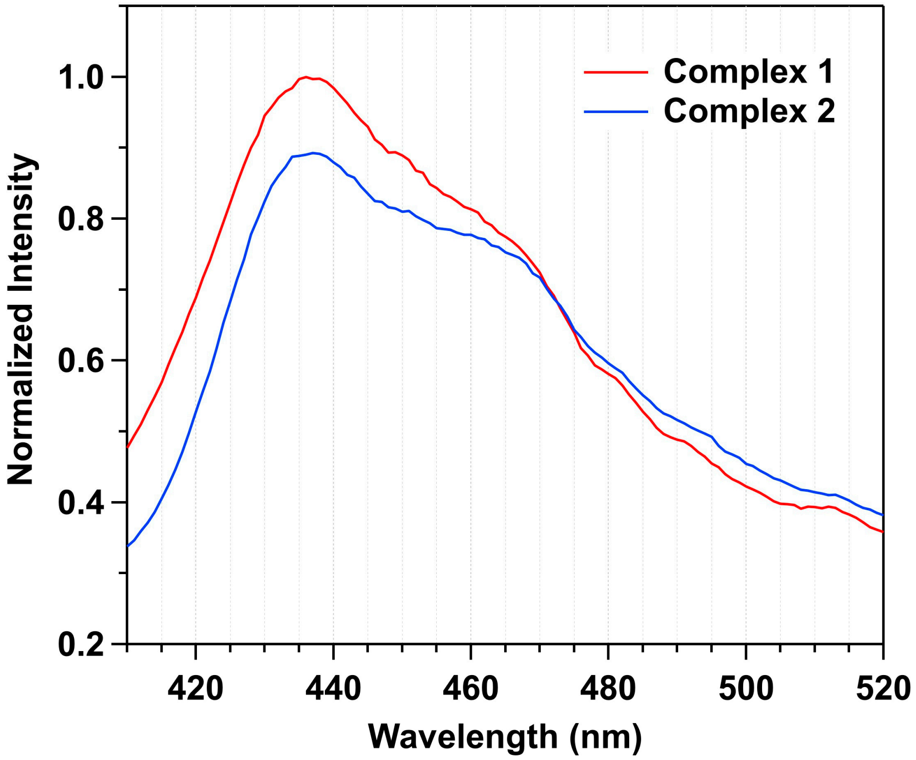

Figure 7. Solid-state normalized fluorescence spectra of complexes **1** and **2** recorded with excitation wavelength, λ_{exc} = 317 nm.

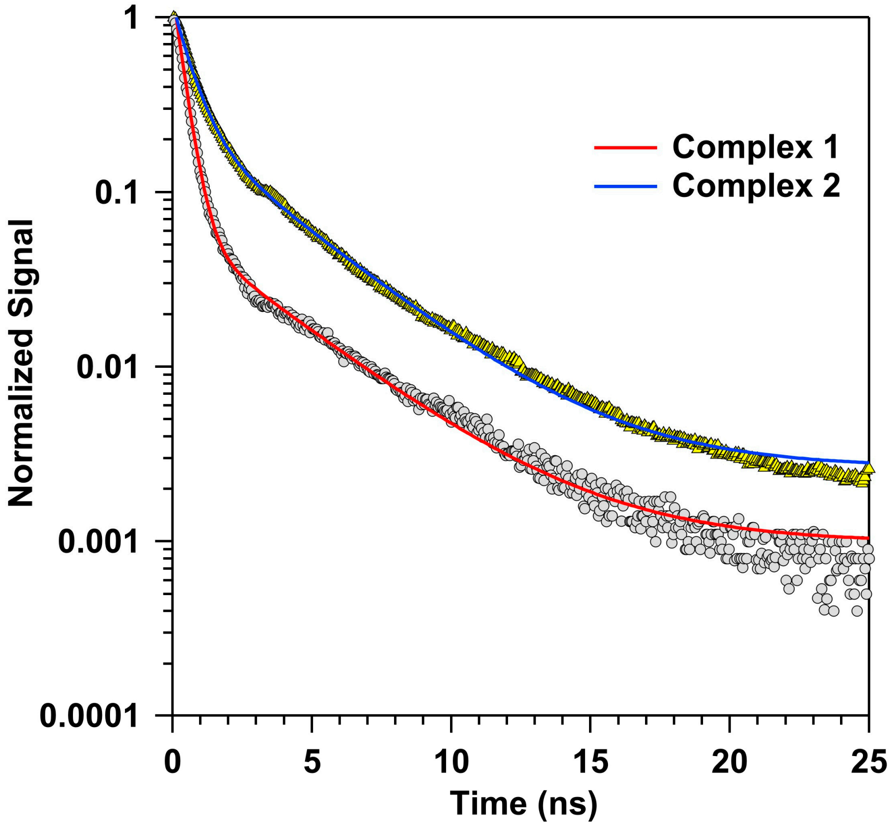

Figure 8. Fluorescence decays of complex **1** (light grey solid circles) and **2** for solid-state (yellow solid triangles), stimulated by the output of a pulsed picosecond diode laser (375 nm). The solid lines represent fit of the data (see the text for details).

The fluorescence temporal profiles were fitted to a double exponential decay presented in Equation (1):

$$F(\mathrm{t}) = \mathrm{Y}_0 + a_1 \times \exp[-(t - t_0)/\tau_1] + a_2 \times \exp[-(t - t_0)/\tau_2] \quad (1)$$

where $F(\mathrm{t})$ is the temporal fluorescence signal, τ_1 and τ_2 are the two decay times, t_0 is the zero-time where decay begins, and a_1 and a_2 are the normalized weighted contributions of the two decay times. For complex **1**, τ_1 and τ_2 were determined to be 0.36 and 3.59 ns, respectively, with an average time τ_{av} = 2.0 ns. The relative contribution of the fast decay to the fluorescence decay was 90%, while the contribution of the slow decay amounted for 10%. For complex **2**, the fast decay was substantially slower compared to complex **1**, τ_1 = 0.62 ns, while the slow decay was similar τ_2 = 3.42 ns. The latter led to a larger average lifetime for **2**, τ_{av} = 2.45 ns (Table 2). As far as the contribution of the two decays in **2** is concerned, significant differences compared to **1** were observed, with the fast and the slow decays contributing for 75 and 25%, respectively. The observed slower fluorescence and the larger contribution of the slow decay in complex **2** are both consistent with the increased dimensionality in the structure of **2** (3-D) compared to the structure of **1** (2-D).

Table 2. Decay times and weighted contributions for **1** and **2**.

Complexes	a_1	τ_1 (ns)	a_2	τ_2 (ns)	τ_{av} (ns)
1	0.904	0.36	0.096	3.59	2.02
2	0.747	0.62	0.253	3.42	2.45

4. Conclusions

In conclusion, in this work we present the synthesis, characterization, and fluorescence properties of two Zn coordination polymers, based upon the use of amino acid Schiff-base ligands. More specifically, we were able to isolate complex $\{[\mathrm{ZnL_1}]\}_{2n}$ (1), which describes a 2D coordination polymer, while upon replacing the metahylalanine amino acid ligand with glycine we were able to isolate complex $\{[\mathrm{ZnL_2}]\cdot 0.33\mathrm{MeOH}\}_{3n}$ (2.0.33MeOH), which describes a 3D coordination polymer. Furthermore, both polymers strongly emit at ~435 nm (λ_{exc} = 317 nm) in solution and solid state, with complex 2 displaying a slightly larger lifetime of τ_{av} = 2.45 ns vs. τ_{av} = 2.02 ns for 1. Finally, we feel this work demonstrates an alternative and easy method for increasing the dimensionality of coordination polymers, upon suitable selection of Schiff-base amino acid ligands.

Supplementary Materials: The following supporting information can be downloaded at: https://www.mdpi.com/article/10.3390/chemistry5030121/s1, Figure S1. FTIR-ATR spectra of **1** and **2**. Figure S2. PXRD patterns for **1** (top) and **2** (bottom). Figure S3. Solutions excitation (λ_{em} = 441 nm) and fluorescence (λ_{ex} = 317 nm) spectra for complexes **1** and **2**. Figure S4. Solid-state fluorescence spectrum of 1-OH-2-naphthaldehyde using 317 nm as excitation wavelength.

Author Contributions: Conceptualization, C.J.M.; methodology, C.J.M. and V.C.P.; formal analysis, C.J.M. and V.C.P.; experimental execution, R.K., P.A.T., and M.-A.I.S.; S.J.D. solved the single-crystal XRD data; writing—original draft preparation, review, and editing, C.J.M. and V.C.P.; supervision, C.J.M. and V.C.P. All authors have read and agreed to the published version of the manuscript.

Funding: This research received no external funding.

Data Availability Statement: Data are available upon request to corresponding authors.

Acknowledgments: This work was carried out in fulfillment of the requirements for the Master thesis of EKA according to the curriculum of the International Graduate Program in "Inorganic Biological Chemistry", which operates at the University of Ioannina within the collaboration of the Departments of Chemistry of the Universities of Ioannina, Athens, Thessaloniki, Patras, and Crete, and the Department of Chemistry of the University of Cyprus.

Conflicts of Interest: The authors wish to declare no conflict of interest.

References

1. Hoskins, B.F.; Robson, R. Infinite Polymeric Frameworks Consisting of Three Dimensionally Linked Rod-like Segments. *J. Am. Chem. Soc.* **1989**, *111*, 5962–5964. [CrossRef]
2. Zhou, H.-C.; Long, J.R.; Yaghi, O.M. Introduction to Metal–Organic Frameworks. *Chem. Rev.* **2012**, *112*, 673–674. [CrossRef] [PubMed]
3. Stock, N.; Biswas, S. Synthesis of Metal-Organic Frameworks (MOFs): Routes to Various MOF Topologies, Morphologies, and Composites. *Chem. Rev.* **2012**, *112*, 933–969. [CrossRef] [PubMed]
4. Howarth, A.J.; Liu, Y.; Li, P.; Li, Z.; Wang, T.C.; Hupp, J.T.; Farha, O.K. Chemical, Thermal and Mechanical Stabilities of Metal–Organic Frameworks. *Nat. Rev. Mater.* **2016**, *1*, 15018. [CrossRef]
5. Saeb, M.R.; Rabiee, N.; Mozafari, M.; Mostafavi, E. Metal-Organic Frameworks (MOFs)-Based Nanomaterials for Drug Delivery. *Materials* **2021**, *14*, 3652. [CrossRef]
6. Zou, D.; Yu, L.; Sun, Q.; Hui, Y.; Tengjisi; Liu, Y.; Yang, G.; Wibowo, D.; Zhao, C.-X. A General Approach for Biomimetic Mineralization of MOF Particles Using Biomolecules. *Colloids Surf. B Biointerfaces* **2020**, *193*, 111108. [CrossRef]
7. Li, H.; Li, L.; Lin, R.-B.; Zhou, W.; Zhang, Z.; Xiang, S.; Chen, B. Porous Metal-Organic Frameworks for Gas Storage and Separation: Status and Challenges. *EnergyChem* **2019**, *1*, 100006. [CrossRef]
8. Dhakshinamoorthy, A.; Li, Z.; Garcia, H. Catalysis and Photocatalysis by Metal Organic Frameworks. *Chem. Soc. Rev.* **2018**, *47*, 8134–8172. [CrossRef]
9. Sohrabi, H.; Ghasemzadeh, S.; Ghoreishi, Z.; Majidi, M.R.; Yoon, Y.; Dizge, N.; Khataee, A. Metal-Organic Frameworks (MOF)-Based Sensors for Detection of Toxic Gases: A Review of Current Status and Future Prospects. *Mater. Chem. Phys.* **2023**, *299*, 127512. [CrossRef]
10. Thorarinsdottir, A.E.; Harris, T.D. Metal–Organic Framework Magnets. *Chem. Rev.* **2020**, *120*, 8716–8789. [CrossRef]
11. Yang, J.; Yang, Y. Metal–Organic Frameworks for Biomedical Applications. *Small* **2020**, *16*, 1906846. [CrossRef]
12. Torresi, S.; Famulari, A.; Martí-Rujas, J. Kinetically Controlled Fast Crystallization of $M_{12}L_8$ Poly-[n]-catenanes Using the 2,4,6-Tris(4-pyridyl)benzene Ligand and $ZnCl_2$ in an Aromatic Environment. *J. Am. Chem. Soc.* **2020**, *142*, 9537–9543. [CrossRef]
13. Martí-Rujas, J.; Elli, S.; Famulari, A. Kinetic trapping of 2,4,6-tris(4-pyridyl)benzene and ZnI_2 into $M_{12}L_8$ poly-[*n*]-catenanes using solution and solid-state processes. *Sci. Rep.* **2023**, *13*, 5605. [CrossRef] [PubMed]
14. Moghadam, P.Z.; Li, A.; Wiggin, S.B.; Tao, A.; Maloney, A.G.P.; Wood, P.A.; Ward, S.C.; Fairen-Jimenez, D. Development of a Cambridge Structural Database Subset: A Collection of Metal–Organic Frameworks for Past, Present, and Future. *Chem. Mater.* **2017**, *29*, 2618–2625. [CrossRef]
15. Brugger, J. Zinc. In *Encyclopedia of Geochemistry*; White, W.M., Ed.; Springer International Publishing: Cham, Switzerland, 2016; pp. 1–4, ISBN 9783319391939.
16. Dumur, F.; Beouch, L.; Tehfe, M.-A.; Contal, E.; Lepeltier, M.; Wantz, G.; Graff, B.; Goubard, F.; Mayer, C.R.; Lalevée, J.; et al. Low-Cost Zinc Complexes for White Organic Light-Emitting Devices. *Thin Solid Film.* **2014**, *564*, 351–360. [CrossRef]
17. Safdar Ali, R.; Meng, H.; Li, Z. Zinc-Based Metal-Organic Frameworks in Drug Delivery, Cell Imaging, and Sensing. *Molecules* **2021**, *27*, 100. [CrossRef] [PubMed]
18. Bahrani, S.; Hashemi, S.A.; Mousavi, S.M.; Azhdari, R. Zinc-Based Metal–Organic Frameworks as Nontoxic and Biodegradable Platforms for Biomedical Applications: Review Study. *Drug Metab. Rev.* **2019**, *51*, 356–377. [CrossRef]
19. McKinlay, A.C.; Morris, R.E.; Horcajada, P.; Férey, G.; Gref, R.; Couvreur, P.; Serre, C. BioMOFs: Metal-Organic Frameworks for Biological and Medical Applications. *Angew. Chem. Int. Ed.* **2010**, *49*, 6260–6266. [CrossRef] [PubMed]
20. Dou, Z.; Yu, J.; Cui, Y.; Yang, Y.; Wang, Z.; Yang, D.; Qian, G. Luminescent Metal–Organic Framework Films As Highly Sensitive and Fast-Response Oxygen Sensors. *J. Am. Chem. Soc.* **2014**, *136*, 5527–5530. [CrossRef]
21. Martí-Rujas, J.; Elli, S.; Sacchetti, A.; Castiglione, F. Mechanochemical synthesis of mechanical bonds in $M_{12}L_8$ poly-[n]-catenanes. *Dalton Trans.* **2022**, *51*, 53–58. [CrossRef]
22. Blackman, A.G.; Schenk, E.B.; Jelley, R.E.; Krenske, E.H.; Gahan, L.R. Five-Coordinate Transition Metal Complexes and the Value of τ_5: Observations and Caveats. *Dalton Trans.* **2020**, *49*, 14798–14806. [CrossRef] [PubMed]
23. Lakowicz, J.R. *Principles of Fluorescence Spectroscopy*, 2nd ed.; Kluwer Academic/Plenum Publishers: New York, NY, USA, 1999; ISBN 0-306-46093-9.